Heat and Mass Transfer 33 (1997) 247–255 © Springer-Verlag 1997

Natural convection in an inclined enclosure with a fluid layer and a heat-generating porous bed

Y.-H. Chen, H.-T. Lin

Abstract Multiple steady-state solutions of natural convection in an inclined enclosure with a fluid layer and a heat-generating porous bed is investigated numerically by the finite volume method. The conservation equations for the porous layer are based on a general flow model which includes both the effects of flow inertia and friction. The flow in fluid layer is modeled by Navier–Stokes equations. The method of pseudo arc-length continuation is adapted in studying the effects of tilt angle on flow pattern and heat transfer. It is found that, in the whole domain of tilt angle, there exist two groups of solutions with quite different flow pattern and heat transfer behavior. The effects of aspect ratio on flow pattern and heat transfer have also been studied.

List of symbols

A	aspect ratio, W/H
C	inertia coefficient
C_p	specific heat [J kg^{-1} K^{-1}]
Da	Darcy number, K/H^2
$\vec{g}$	gravitational acceleration [m s^{-2}]
H	vertical length of the enclosure [m]
h	heat transfer coefficient [W m^{-2} K^{-1}]
K	permeability of the porous medium [m^2]
k	thermal conductivity of fluid [W m^{-1} K^{-1}]
Nu	global Nusselt number, $h\Gamma/k$
P	pressure [Pa]
Pr	Prandtl number, ν/α
Ra	Rayleigh number, $g\beta T^* H^3/\nu\alpha$
R_k	thermal conductivity ratio, k_{eff}/k
$\dot{q}$	volumetric heat generating in porous layer [W m^{-3}]
T	temperature [K]
T^*	characteristic temperature $\dot{q}H^2/k$ [K]
T_m	mean temperature at the interface [K]
T_w	enclosure wall temperature [K]
U	dimensionless velocity in x direction
v	velocity vector (u, v) [m s^{-1}]
V	dimensionless velocity in y direction
V	dimensionless velocity vector (U, V)
W	horizontal length of the enclosure [m]
x, y	horizontal and vertical coordinates [m]
X, Y	dimensionless coordinates x/W, y/H

Greek symbols

α	thermal diffusivity [m^2 s^{-1}]
β	thermal expansion coefficient of fluid [K^{-1}]
Γ	boundaries of the enclosure [m]
ε	porosity
θ	dimensionless temperature
θ_m	dimensionless mean temperature at the interface
λ	binary parameter
μ	viscosity [kg m^{-1} s^{-1}]
ν	kinematic viscosity [m^2 s^{-1}]
ρ	fluid density [kg m^{-3}]
φ	tilt angle [deg]
ψ	stream function [m^2 s^{-1}]
ω	vorticity [s^{-1}]

Subscripts

c	center of the enclosure
eff	effective thermophysical properties
f	fluid layer
m	mean value
p	porous layer

Received on 04 March 1997

H.-T. Lin Y.-H. Chen
Department of Chemical Engineering
National Central University
Chungli, Taiwan 320, R. O. C.

Correspondence to: H.-T. Lin

This work was supported by a grant NSC85-2214-E008-015 from the National Science Council of Republic of China.

1 Introduction

Buoyancy-driven convection in a porous enclosure can be encountered in many engineering and environmental applications. For example, cooling of buried nuclear wastes, transport of heat within the earth crust, and catalitical chemical reaction in a batch reactor. Therefore, a considerable amount of investigations on this subject have been performed over the last 30 years.

For an enclosure filled with porous material, several investigations [1–4] have focused on the phenomenon of natural convection from volumetric heat generating. Most of these investigations deal with uniform heat generation in the cavity and isothermal boundaries along the vertical or horizontal walls. A detail discussion on bifurcation with respect to the Rayleigh number for a system with uniform heat generation has been made by Weinitschke et al. [5]. Both symmetric and asymmetric solution branches were studied over a wide range of Rayleigh number. Vilijoen and Hlavacek [6], and Subramanian and Balakotaiah [7] worked with non-uniform heating rate determined by chemical reaction. They also provided with bifurcation diagrams.

A system of inclined porous layer has also been noticed. Inaba et al. [8] performed an experimental study of a sloped porous layer heated from below with constant temperature. They reported a correlation equation between the Nusselt number and the modified Rayleigh number for any inclined angles. The same system was also studied numerically by Moya et al. [9]. Flow of multiple cells and multiple steady states have been found in their research. The same problem but with uniform wall flux has also been studied numerically and analytically by Vasseur et al. [10], and by Sen et al. [11] under the assumption of parallel flow. According to the report of Sen et al., three different steady states can be found for unicellular convection within a small tilt angle when the Rayleigh number is larger than a critical value.

Natural convection in an enclosure with a porous bed and an overlaying fluid also attracted some interests [12–17]. A numerical and experimental study of this system has been reported by Beckermann et al. [13]. They added the Brinkman term for friction force, and the Forchheimer term for inertia effects. The numerical solution were validated by the temperature measurements and interferometric results. System of fluid layer overlaying a uniform heat generating porous bed with three insulated boundaries and a top cold wall was investigated numerically by Poulikakos [17]. According to his study with a general flow model, two or four even six cells can be obtained for different aspect ratios.

In the present work, we consider a system similar to that has been studied by Poulikakos, except that the present cavity is inclined and all the boundaries are isothermal walls. We concentrate our attention on the effect of tilt angle on the flow pattern and heat transfer performance of natural convection in the enclosure. In addition, we intend to find multiple steady-state solutions of this system by using pseudo arc-length continuation technique [18].

2 Formulations

As shown in Fig. 1, consider a rectangular enclosure which is tilted at an angle φ with respect to the horizontal. The enclosure is bounded by impermeable isothermal walls and divided equally into a fluid layer and a porous layer. The fluid layer is filled with Newtonian fluid of constant viscosity μ and thermal conductivity k, while the porous layer is packed with a homogenous porous medium of effective thermal conductivity k_{eff} and viscosity μ_{eff}.

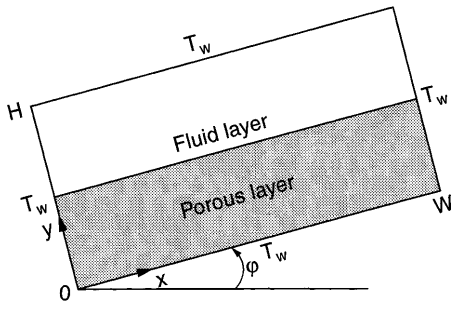

Fig. 1. Physical model and coordinate system

Thermal energy of volumetric rate $\dot{q}$ has been generated constantly and uniformly in the porous layer, which may arises from a catalytic reaction or a heat-release adsorption process.

In the enclosure, the buoyancy-induced flow arising from heat generation is assumed to be steady, laminar, and two-dimensional. Besides, the physical properties of the fluid and the porous material are assumed to be constant except that the Boussinesq approximation is invoked to model the density variation in the buoyancy term.

For the fluid layer, the governing equations are:

$$\nabla \cdot \mathbf{v} = 0 \tag{1}$$

$$\rho(\mathbf{v} \cdot \nabla)\mathbf{v} = \mu\nabla^2\mathbf{v} - \nabla P + \rho\vec{g}\beta(T - T_w) \tag{2}$$

$$\rho c_p(\mathbf{v} \cdot \nabla)T = k\nabla^2 T \ . \tag{3}$$

In the porous layer, the fluid-saturated porous medium is assumed to be homogeneous, isotropic and in local thermal equilibrium with the fluid. The flow in porous region is modeled by Brinkman-Forchheimer-extended Darcy model which includes both inertia and viscous terms. This model is based on a general flow model and has been derived semi-empirically [19]. The conservation equations for the porous layer are:

$$\nabla \cdot \mathbf{v} = 0 \tag{4}$$

$$\frac{\rho}{\varepsilon^2}(\mathbf{v} \cdot \nabla)\mathbf{v} = \mu_{\text{eff}}\nabla^2\mathbf{v} - \nabla P - \left[\frac{\mu}{K} + \frac{C}{\sqrt{K}}|\mathbf{v}|\right]\mathbf{v} + \rho\vec{g}\beta(T - T_w) \tag{5}$$

$$\rho c_p(\mathbf{v} \cdot \nabla)T = k_{\text{eff}}\nabla^2 T + \dot{q} \tag{6}$$

where $|\mathbf{v}| = \sqrt{u^2 + v^2}$ is the flow intensity; ε and K are, respectively, the porosity and permeability of the porous medium; k_{eff} and μ_{eff} are effective thermal conductivity and effective viscosity of the porous medium.

Since the four bounding walls are solid and isothermal, the boundary conditions for the above equations are as follows:

$$u = 0, \quad v = 0, \quad T = T_w \quad \text{at } x = 0 \text{ and } x = W \tag{7a}$$

$$u = 0, \quad v = 0, \quad T = T_w \quad \text{at } y = 0 \text{ and } y = H. \tag{7b}$$

At the interface of the fluid and the porous layers, the following matching conditions must be satisfied:

$$u_f = u_p, \quad v_f = v_p, \quad \tau_f = \tau_p, \quad P_f = P_p, \quad T_f = T_p$$

$$\mu\left(\frac{\partial u}{\partial y} + \frac{\partial v}{\partial x}\right)\bigg|_{y=y_f^+} = \mu_{\text{eff}}\left(\frac{\partial u}{\partial y} + \frac{\partial v}{\partial x}\right)\bigg|_{y=y_p^-} \tag{8}$$

$$T_f = T_p, \qquad k\frac{\partial T}{\partial y}\bigg|_{y=y_f^+} = k_{\text{eff}}\frac{\partial T}{\partial y}\bigg|_{y=y_p^-}.$$

These matching conditions, proposed by Neale and Nader [20], describe the continuation of the shear stress, velocity components, temperature, and heat flux. The inclusion of the Brinkman term in the momentum equation for the porous media makes it possible to satisfy the above matching condition at porous-fluid interface.

From the continuation of physical quantities, Beckermann [13] suggested that the conservation equa-

tions for the fluid and porous layers can be combined into a single set of equations by introducing the binary parameter:

$$\lambda = \begin{cases} 0 & \text{in the fluid layer} \\ 1 & \text{in the porous layer} \end{cases}. \tag{9}$$

In order to normalize all the variables in Eqs. (1)–(8), we define the following dimensionless variables:

$$(X, Y) = \left(\frac{x}{W}, \frac{y}{H}\right); \quad (U, V) = \left(\frac{uW}{\alpha}, \frac{vH}{\alpha}\right);$$
$$T^* = \frac{\dot{q}H^2}{k}; \qquad \theta \equiv \frac{T - T_w}{T^*}; \tag{10}$$
$$\mathrm{Ra} = \frac{g\beta T^* H^3}{v\alpha}; \quad \mathrm{Da} = \frac{K}{H^2}.$$

In addition, to eliminate the pressure term in the momentum equations and for numerical convenience, the stream function and vorticity have been introduced as follow:

$$U = -A\frac{\partial \psi}{\partial Y}; \quad V = \frac{1}{A}\frac{\partial \psi}{\partial X}; \quad \omega = \frac{1}{A}\left(\frac{\partial U}{\partial Y} - \frac{\partial V}{\partial X}\right). \tag{11}$$

By using the variables defined in Eqs. (8)–(11), the two sets of governing equations, Eqs. (1)–(3) and Eqs. (4)–(6), can be combined and reduced to the following:

$$\nabla^2 \psi = -\omega A^2 \tag{12}$$

$$\left(1 - \lambda + \frac{\lambda}{\varepsilon^2}\right)\left(\frac{U}{A}\frac{\partial \omega}{\partial X} + AV\frac{\partial \omega}{\partial Y}\right)$$
$$= \frac{\mathrm{Pr}}{A}\nabla_A^2 \omega + \mathrm{Pr}\ \mathrm{Ra}\left(A\frac{\partial \theta}{\partial Y}\sin\varphi - \frac{\partial \theta}{\partial X}\cos\varphi\right) \tag{13}$$
$$- \lambda\frac{\mathrm{Pr}}{\mathrm{Da}}A\omega + \frac{\lambda AC}{\sqrt{\mathrm{Da}}}\left(\frac{\partial}{\partial X}|\mathbf{V}|V - \frac{\partial}{\partial Y}|\mathbf{V}|U\right)$$

$$U\frac{\partial \theta}{\partial X} + A^2 V\frac{\partial \theta}{\partial Y} = (\lambda(R_k - 1) + 1)\nabla_A^2 \theta + \lambda A^2 \tag{14}$$

where ∇_A^2 is defined as

$$\nabla_A^2 \equiv \frac{\partial^2}{\partial X^2} + A^2\frac{\partial^2}{\partial Y^2} \tag{15}$$

and the thermal conductivity ratio R_k is the ratio of the fluid conductivity to the effective conductivity of porous medium.

At the boundaries, the dimensionless boundary condition is

$$y = 0, \quad \theta = 0. \tag{16}$$

During the procedure of equation unification, the effective viscosity μ_{eff} has been set to be equal to the fluid viscosity. For most porous medium, this approximation provides good agreement with experimental data [21]. Besides, Lauriat and Prasad [22] also performed a numerical analysis on the effects of viscosity ratio. They conclude that in the range of $0.5 < \mu_{\mathrm{eff}}/\mu < 2.5$, the variation in the viscosity ratio has little influence on the Darcy–Brinkman solutions if $\mathrm{RaDa} < 10^3$ and $\mathrm{Da} < 10^{-5}$.

3 Numerical procedure

Equations (12)–(14) were discretized into algebraic, finite difference equations by using the control volume formulations [23]. This method assures that the conservation laws are obeyed over arbitrarily large or small control volume. The harmonic mean formulation was used to obtain the interface diffusion coefficients between two control volumes. The nonlinear Forchheimer term in the momentum equations of porous layer was split into two parts, i.e. $\frac{\lambda AC}{\sqrt{\mathrm{Da}}}|\mathbf{V}|\omega + \frac{\lambda C}{\sqrt{\mathrm{Da}}}\left(V\frac{\partial|\mathbf{V}|}{\partial X} + U\frac{\partial|\mathbf{V}|}{\partial Y}\right)$. The first part was combined with the Darcy term and numerically treated as an unknown with a non-linear coefficient. The other part that includes first-order derivatives of flow intensity was modeled as a source term.

As a first step of the solution procedure, the governing equations and the continuation equation have been discretized. Then, the resulting nonlinear coupled algebraic equations were solved simultaneously by using Newton–Raphson method for all variables. The Jacobin matrix used in Newton's iteration is calculated numerically by the forward difference, and the resulting linear equations are solved by GMRES method with ILU(0) precondition. GMRES is an iterative technique introduced by Saad and Schultz [24] for solving general large sparse asymmetric linear system of equations by minimizing the 2-norm of the residual vector. It has the feature of robustness, less CPU time consuming and memory saving. This sparse matrix package has also been used widely in fluid flow computation.

In order to locate the solution from one to the other, the pseudo arc-length continuation [18] is adapted in the present study. Besides, for many nonlinear systems there may exist a turning or a bifurcation point in parameter space. To such a point, Newton's method may fail to get a convergent solution because of the singular Jacobian matrix. To defeat this, the technique of continuation is usually helpful. The idea of continuation is to trace the solutions alone a branch through an arc-length s by including an additional equation for the continuation parameter p:

$$(\mathbf{f}(s) - \mathbf{f}(s_0))^T \cdot \left.\frac{\partial \mathbf{f}}{\partial s}\right|_{s_0} + (p(s) - p(s_0))^T \cdot \left.\frac{\partial p}{\partial s}\right|_{s_0} - (s - s_0) = 0 \tag{17}$$

where $\mathbf{f} = (\psi, \omega, \theta)^T$, the arc-length $s \equiv \|(\mathbf{f}, p)^T\|_2$ and $(s - s_0)$ is the step size along the solution branch. The aim of the present study is focused on the incline of the system, hence, the tilt angle φ is chosen as the continuation parameter.

According to the study of Nishmura [16], the thickness of the region near the interface, δ, in which the flow in the porous region is dominated by viscous force is roughly estimated as $\delta/W \sim \sqrt{\mathrm{Da}}$. In the region near the interface, the grid size should be smaller than $\sqrt{\mathrm{Da}}$. Otherwise, a remarkable error would probably arise in the numerical solution, and the resulting flow patterns may be quite different. In the present study, the grid size near the interface is generated according to this law, and non-uniform mesh is calculated by the stretch function mentioned

in Ref. [25]. It was found that a grid of 60×30 yielded results not significantly different from a grid of 80×40 for the case of $A = 2$. Hence, the grid number used in the present study is 80×40. The grid is dense near the boundary and interface.

The validation of the numerical code is very important and difficult. In order to verify the solution, a comparison with the previous works is necessary. Sen, Vasseur and Robillard [11] propounded analytical solution for a tilted slender rectangular cavity filled with porous medium and heated uniformly from the bottom. The system was resolved by the numerical code developed in the present study to assure the correctness of the numerical approach. By using the same flow model (Darcy model), and the same aspect ratio ($A = 4$), the numerical results agree well with the analytical solution. The maximum error is less than 0.5%.

4
Results and discussion

4.1
System parameters and variables

From Eqs. (13) and (14), we know that natural convection in an enclosure with fluid and porous layers is affected by several dimensionless groups: the Rayleigh number Ra, the Prandtl number Pr, the Darcy number Da, the aspect ratio A, and the thermal conductivity ratio R_k. In addition, the porosity ε, the inertia coefficient C, and the tilt angle φ also influence the flow pattern and heat transfer of the system.

The effect of the porosity on flow is not significant as shown in Table 1 for a system of $\varphi = 90°$. In the range of $0.1 < \varepsilon < 1$, the stream function at the center of the enclosure, ψ_c, changes within 3 percent. The little effect of the porosity also appear in the numerical data of Lauriat and Prasad [22] which varying ε from 0.1 to 0.9 and have small change in Nusselt number. This is because that the porosity appear only in the convective term which is not significant for the porous media [26].

In the present study, we focus our attention on the effects of tilt angle and the Rayleigh number on flow pattern and heat transfer performance. Hence, the other parameters were specified as: $\mathrm{Pr} = 0.7$ and $A = 2$. The inertia coefficient C is chosen as 0.55 from Ergun model.

4.2
Two groups of solutions

The stream function at the center of the enclosure, ψ_c, is chosen to characterize the flow. The variation of ψ_c over the whole domain of tilt angle is shown in Fig. 2 for $A = 2$ and $\mathrm{Ra} = 10^6$. There are two groups of different $\psi_c - \varphi$ relationship shown as solid and dashed lines in Fig. 2. For the purpose of clarity, these two groups have been shown separately in Figs. 3 and 4 for $A = 2$ and some selected values of Ra. Due to the symmetry (as shown in Fig. 2), only the curves in the region of $0° \le \varphi \le 180°$ is needed to be shown.

Table 1. Stream function at the center of the enclosure, ψ_c, for $A = 2$ and $\varphi = 90°$

ε	$\mathrm{Da} = 10^{-4}$		$\mathrm{Da} = 10^{-7}$	
	$\mathrm{Ra} = 10^5$	$\mathrm{Ra} = 10^6$	$\mathrm{Ra} = 10^5$	$\mathrm{Ra} = 10^6$
0.1	−4.008	−12.65	−3.938	−12.15
0.2	−3.986	−12.35	−3.938	−12.16
0.4	−3.981	−12.31	−3.938	−12.16
0.8	−3.979	−12.30	−3.938	−12.16
1.0	−3.979	−12.30	−3.938	−12.16

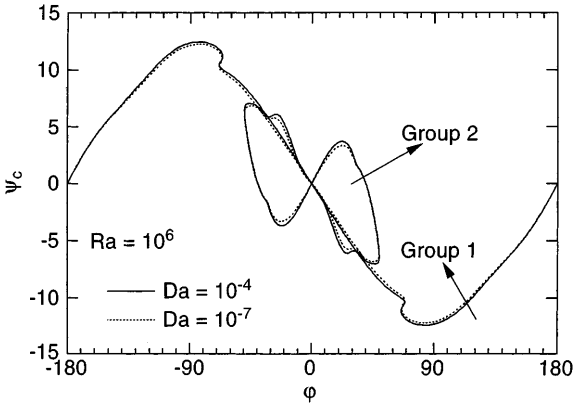

Fig. 2. Variations of ψ_c with tilt angle, $A = 2$, $\mathrm{Ra} = 10^6$

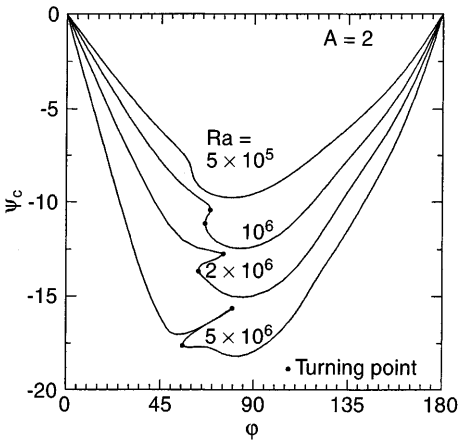

Fig. 3. Variations of ψ_c with tilt angle for the first group of solutions, $A = 2$

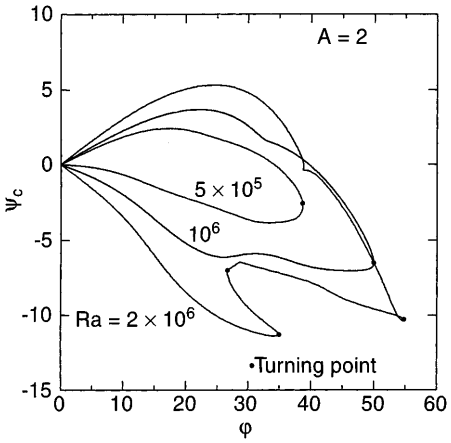

Fig. 4. Variations of ψ_c with tilt angle for the second group of solutions, $A = 2$

It is also shown in Fig. 2 that the Darcy number has weak effect on ψ_c. A variation of Da from 10^{-4} to 10^{-7} changes ψ_c slightly. Hence, all the numerical simulation performed here are based on $\mathrm{Da} = 10^{-4}$.

Figure 3 presents the variations of ψ_c for the first group between $\varphi = 0^\circ$ (horizontal) and $\varphi = 180^\circ$. As can be seen from Fig. 3, ψ_c reaches a minimum at tilt angles about 80° for a specified Ra. It is worthy to note that, on each curve of Ra greater than 10^6, there are two turning points which have been indicated as a dot in Fig. 3. The angles correspond to turning point is named as the turning angles. The turning angles for the case of $A = 2$ and $\mathrm{Da} = 10^{-4}$ have been listed in Table 2.

The second group of $\psi_c - \varphi$ relationship is shown in Fig. 4. Each branch of this group is a closed loop between $\varphi = 0^\circ$ and a extreme turning angle. The turning angles of the second group for some specified Ra have also been listed in Table 2.

As can be seen from Fig. 4, the branches of $\mathrm{Ra} = 5 \times 10^5$ and 10^6 are simple in shape. However, the branch of $\mathrm{Ra} = 2 \times 10^6$ or larger is quite complicated.

4.3
Flow patterns and temperature fields

Flow patterns (stream lines) for some representative tilt angles ($\varphi = 0^\circ, 45^\circ, 68^\circ, 90^\circ, 135^\circ, 180^\circ$ and 315°) have been plotted in Figs. 5–11 for $A = 2$, $\mathrm{Ra} = 10^6$ and $\mathrm{Da} = 10^{-4}$. The positive and negative signs in the center of the cells represent clockwise and counter-clockwise circulation, respectively.

Temperature fields (isotherms) for these angles have also been presented in Figs. 5–10.

Table 2. Turning angles for the first and second groups, $A = 2$, $\mathrm{Da} = 10^{-4}$

	$\mathrm{Ra} = 5 \times 10^5$	$\mathrm{Ra} = 10^6$	$\mathrm{Ra} = 2 \times 10^6$	$\mathrm{Ra} = 5 \times 10^6$
1st group	–	68.84°	75.23°	79.90°
		66.31°	63.20°	55.67°
2nd group	38.71°	49.96°	56.79°	53.03°
			34.98°	and many
			26.72°	others

(1) Flow patterns for $\varphi = 0^\circ$

For a horizontal enclosure ($\varphi = 0^\circ$) with $\mathrm{Ra} = 10^6$, three steady solutions can be found. The flow patterns of these solutions are shown on the left side of Figs. 5a–c, while the temperature fields are shown on the right.

Figure 5a shows a two-cells flow pattern which belongs to the first group of solutions. In the region near the central line, the fluid rises from the porous layer to the fluid layer. It goes away from the center and then falls down along the side boundaries.

The flow pattern shown in Fig. 5b belongs to the second group of solutions. It consists of two primary cells and two secondary cells. At the region near the central line, the primary cells bring fluid upward while the secondary cells bring fluid downward.

The flow pattern shown in Fig. 5c also belongs to the second group of solutions. It consists of four cells. The outer cells are larger than the inner ones. The fluid flows downward near the central line and the two side boundaries.

As can be seen from the right side of Figs. 5a–c, the temperature fields depend strongly on the flow patterns. For the patterns shown in Figs. 5a and 5b, the maximum temperature is located near the center of the enclosure. For the four cells pattern shown in Fig. 5c, the maximum temperature is located in two different places in the porous region.

(2) Flow patterns for $\varphi = 45^\circ$

As shown in Fig. 6, there are also three solutions for an enclosure with tilt angle $\varphi = 45^\circ$ and $\mathrm{Ra} = 10^6$. The one belongs to the first group of solutions is a two-cells flow

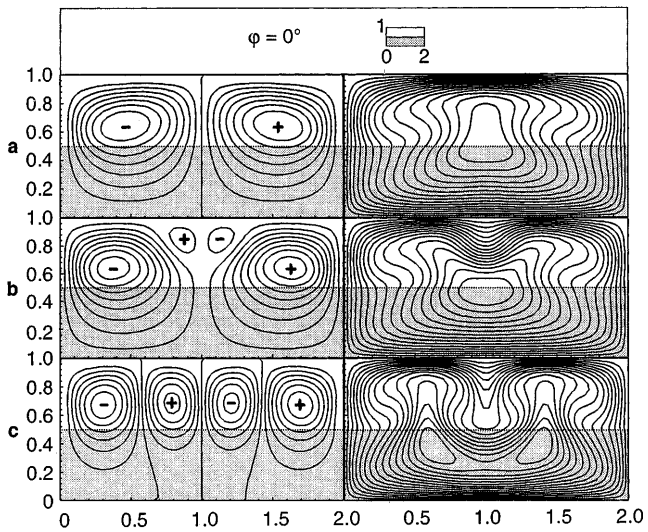

Fig. 5a–c. Stream lines and isotherms for $\varphi = 0^\circ$. **a** $\psi_c = 0$, $\Delta\psi = 1.470$, $\Delta\theta = 2.614 \times 10^{-3}$; **b** $\psi_c = 0$, $\Delta\psi = 1.1249$, $\Delta\theta = 2.991 \times 10^{-3}$; **c** $\psi_c = 0$, $\Delta\psi = 1.120$, $\Delta\theta = 2.409 \times 10^{-3}$

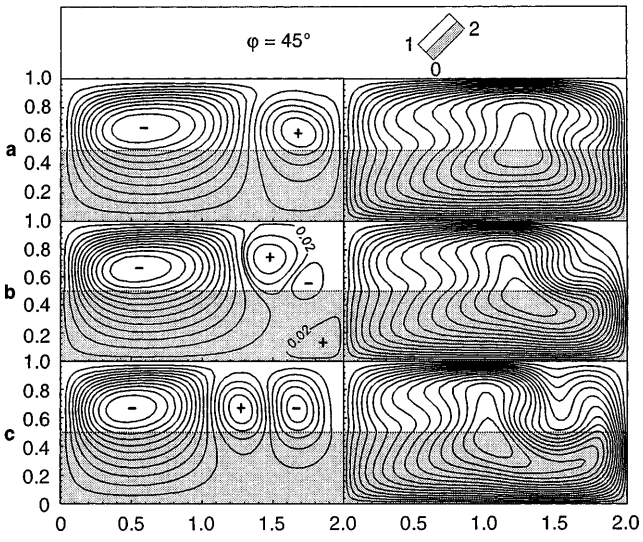

Fig. 6a–c. Stream lines and isotherms for first solution group at $\varphi = 45^\circ$. **a** $\psi_c = -7.763$, $\Delta\psi = 1.275$, $\Delta\theta = 2.759 \times 10^{-3}$; **b** $\psi_c = -6.926$, $\Delta\psi = 1.060$, $\Delta\theta = 3.017 \times 10^{-3}$; **c** $\psi_c = -2.614$, $\Delta\psi = 1.020$, $\Delta\theta = 2.766 \times 10^{-3}$

pattern shown in Fig. 6a. The fluid flows downward along the side boundaries into porous layer. It is similar to Fig. 5a except that the right cell is smaller than the left one.

The flow patterns shown in Figs. 6b and 6c belong to the second group of solutions. They are more complicated than the previous one.

The flow shown in Fig. 6b consists of a main counter-clockwise cell and three much smaller secondary cells. One of the secondary cells is in the porous layer, and other two are essentially in the fluid layer.

The flow pattern shown in Fig. 6c consists of three cells. A clockwise cell lies between two counter-clockwise cells.

(3) Flow patterns for $\varphi = 68^\circ$

As has been mentioned, there are two turning points for Ra greater than 10^6 in the first group of solutions. Three different solutions for a specified Ra can be found at any angle between the two turning angles. The basic flow pattern of these solutions is a main circulation with a secondary cell on the right side, as can be seen from Fig. 7 for $\varphi = 68^\circ$ and $\mathrm{Ra} = 10^6$.

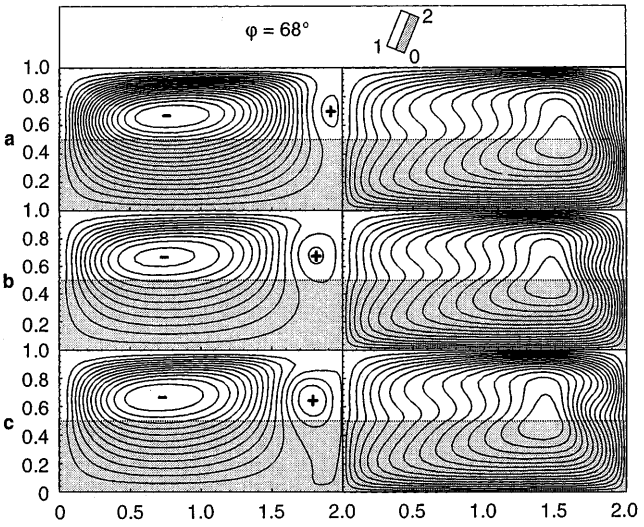

Fig. 7a–c. Stream lines and isotherms for first solution group at $\varphi = 68^\circ$ **a** $\psi_c = -11.68$, $\Delta\psi = 0.800$, $\Delta\theta = 2.983 \times 10^{-3}$; **b** $\psi_c = -10.65$, $\Delta\psi = 0.910$, $\Delta\theta = 2.964 \times 10^{-3}$; **c** $\psi_c = -10.27$, $\Delta\psi = 1.079$, $\Delta\theta = 2.912 \times 10^{-3}$

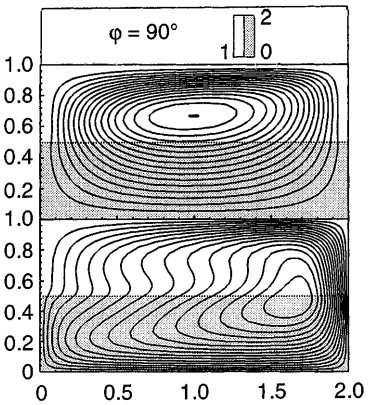

Fig. 8. Stream lines and isotherms for first solution group at $\varphi = 90^\circ$: $\psi_c = -12.35$, $\Delta\psi = 0.962$, $\Delta\theta = 2.945 \times 10^{-3}$

(4) Flow pattern for $\varphi = 90^\circ$

Figure 8 shows that, for a vertical enclosure ($\varphi = 90^\circ$) with $\mathrm{Ra} = 10^6$, the flow pattern is simply a single cell. In the heat-generating porous layer the fluid flows upward. While in the fluid layer, it flows downward.

(5) Flow pattern for $\varphi = 135^\circ$

A single cell flow is found and shown in Fig. 9 for $\varphi = 135^\circ$. This pattern is like the pattern shown in Fig. 8, except that the stream lines are denser on the upper corner of the fluid layer.

(6) Flow pattern for $\varphi = 180^\circ$

The flow pattern for $\varphi = 180^\circ$ shown in Fig. 10 is similar to that shown in Fig. 5a for $\varphi = 0^\circ$. Both of them consists of two symmetry cells with reverse circulation. In addition, fluid near the central region flows upward for both cases. However, the intensity of the cell for $\varphi = 180^\circ$ is much smaller (about an order) than that for $\varphi = 0^\circ$.

The temperature field shown in Fig. 10 indicates clearly that heat conduction is a dominating process, and the maximum temperature is located in the porous layer.

(7) Flow patterns for $\varphi = 315^\circ$

Figure 11 shows the flow patterns of the three solutions for $\varphi = 315^\circ$ (-45°). This figure is almost the same as Fig. 6

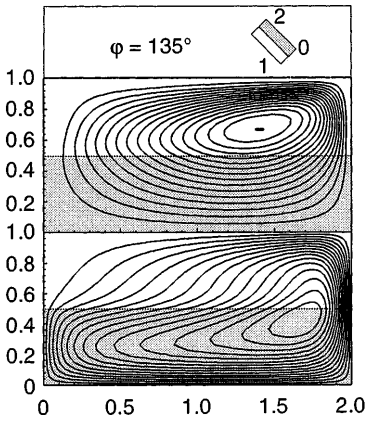

Fig. 9. Stream lines and isotherms for $\varphi = 135^\circ$: $\psi_c = -7.696$, $\Delta\psi = 0.684$, $\Delta\theta = 3.093 \times 10^{-3}$

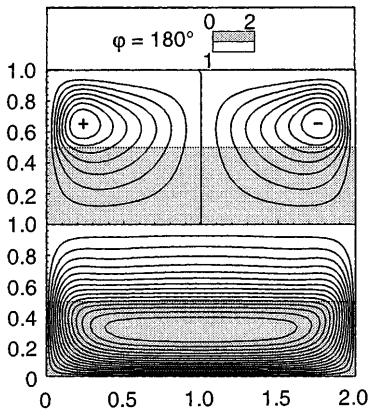

Fig. 10. Stream lines and isotherms for first solution group at $\varphi = 180^\circ$, $\psi_c = 0$, $\Delta\psi = 0.350$, $\Delta\theta = 3.275 \times 10^{-3}$

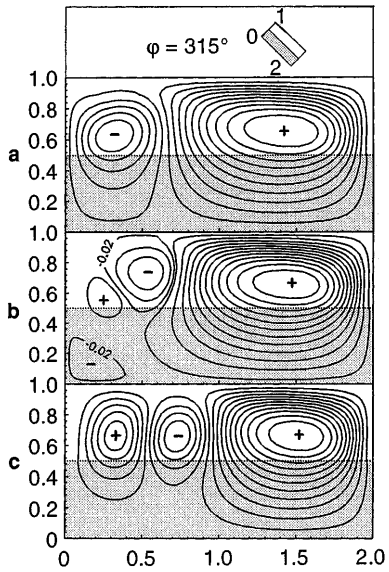

Fig. 11a–c. Stream lines for first solution group at $\varphi = 315°$. **a** $\psi_c = 7.763$, $\Delta\psi = 1.275$; **b** $\psi_c = 6.926$, $\Delta\psi = 1.060$; **c** $\psi_c = 2.614$, $\Delta\psi = 1.020$

for $\varphi = 45°$, except that they are with reverse flow circulation and reverse location of cells. This situation can be found for the cases of any two symmetric angles (e.g., $\varphi = 90°$ and 270°; $\varphi = 135°$ and 225°, etc.).

An inspection on all the flow patterns shown in Figs. 5–11 reveals that the center of the cells are located in the fluid layer. In addition, the stream lines are denser in this layer. It means that most of the flow activities take place in the fluid layer.

4.4
Global Nusselt number

In order to express the heat transfer rate, the global Nusselt number is introduced as follows:

$$\mathrm{Nu} = \frac{h\Gamma}{k} = \frac{1}{T_m - T_w}\int_\Gamma \frac{\mathrm{d}T}{\mathrm{d}n}\,\mathrm{d}\Gamma \qquad (18)$$

where Γ represents the boundary of the enclosure; n the normal vector of the boundary; and T_m the mean temperature at the interface of the fluid and porous layers. Since the total heat flow out of the boundaries is equal to the heat generation inside the porous layer, Eq. (18) can be simplified as:

$$\mathrm{Nu} = \frac{A}{2\theta_m} \qquad (19)$$

where $\theta_m = (T_m - T_w)/T^* = (T_m - T_w)(k/\dot{q}H^2)$ is a dimensionless mean temperature.

4.5
Variations of Nu with φ for the first group

Variations of the global Nusselt number with φ and Ra are presented in Fig. 12 for the first group of solutions. Heat transfer of this group is resulted from the flow pattern of either a single cell or two cells.

As has been shown in Fig. 12 that, for a fixed Ra, the system reaches a maximum value of Nu around $\varphi = 115°$

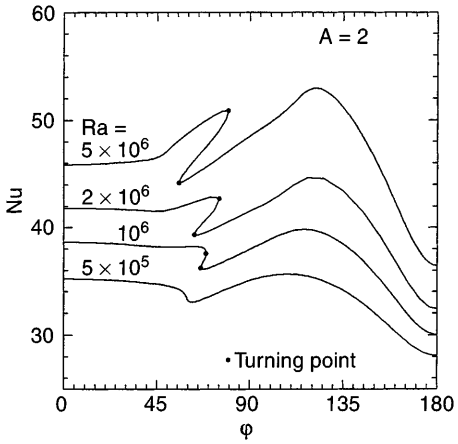

Fig. 12. Variations of the global Nusselt number with tilt angle for the first group of solutions

at which the porous layer is turned to the upper side of the enclosure. At this angle, heat transfer by conduction and convection has been adjusted to a best heat transfer result. A further increase in tilt angle will increase the conduction rate but decrease the rate of convection, and thus reduce the overall heat transfer performance.

It is worthy to note from Fig. 12 that the global Nusselt number increases significantly around the turning angles. This is due to a stronger secondary flow covering the fluid and the porous layers.

The dependence of the Nusselt number on the tilt angle is very weak when the angle is less than 45°, as shown in Fig. 12. At small tilt angles the intensity of the secondary flow is strong enough to bring heat away efficiently by convection. A further increase in the strength of the secondary flow by reducing tilt angle will not significantly change the average interfacial temperature and the Nusselt number.

4.6
Variations of Nu with φ for the second group

The effect of the tilt angle on Nu for the second group of solutions is shown in Fig. 13. Each curve of Nu for a specified Ra can be divided into the upper part and the lower part, which arise from two different types of flow patterns. The Nusselt number above the turning point corresponds to the flow patterns shown in Figs. 5c and 6c. Higher Nu is resulted from the effective flow circulation. In these flow patterns, all the cells circulate across both the fluid and the porous layers. While the Nusselt number below the turning point corresponds to the patterns shown in Figs. 5b and 6b.

4.7
The effects of aspect ratio

As has just been mentioned, the flow patterns and heat transfer performance of the present system are affected strongly by the tilt angle and Ra. In addition, they are also dependent on the aspect ratio of the enclosure.

To examine the effects of aspect ratio, we take the horizontal enclosure ($\varphi = 0°$) as a typical example.

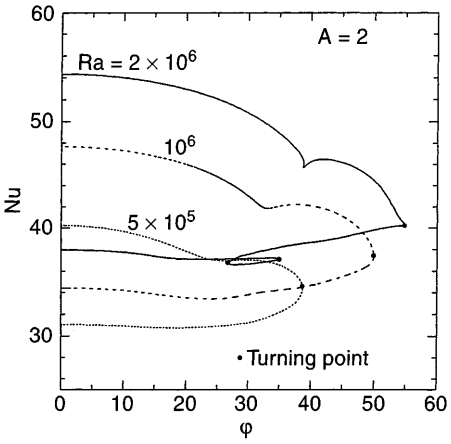

Fig. 13. Variations of the global Nusselt number with tilt angle for the second group of solutions

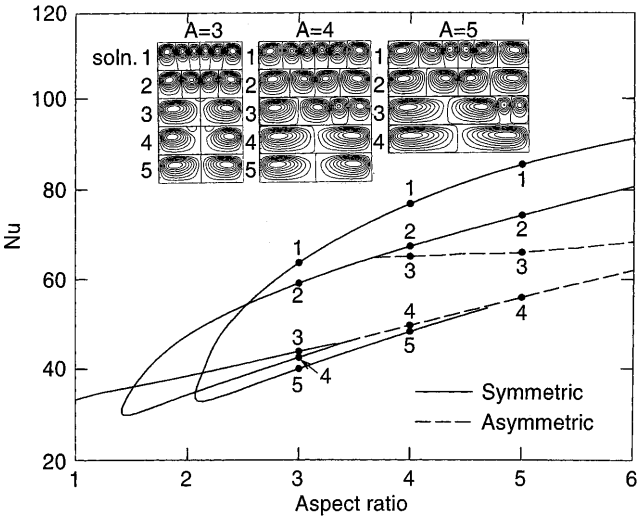

Fig. 14. Variations of the flow patterns and global Nusselt number with aspect ratio

The flow patterns of the multiple steady solutions for the horizontal enclosures of $A = 3$, 4 and 5 have been shown in Fig. 14, while those for $A = 2$ has been presented in Fig. 5. It is seen from these figures that the flow patterns with 2, 4 and 6 symmetric cells as well as 2 and 4 asymmetric cells can be found for $\varphi = 0^\circ$ and $\mathrm{Ra} = 10^6$. As the asymmetric patterns exist conjugately, only one of the pair is shown on this figure.

The effects of aspect ratio on the global Nusselt number are also presented in Fig. 14 for $\varphi = 0^\circ$ and $\mathrm{Ra} = 10^6$. This figure shows that the global Nusselt number increases with increasing aspect ratio for flows of similar pattern with the same number of cells.

A comparison on the heat transfer performance for the multiple solutions of a specified aspect ratio ($A = 3, 4$ and 5) has also been made. It is seen that the global Nusselt number increases with increasing number of cells.

5 Conclusion

The effects of tilt angle on natural convection in an enclosure divided into a fluid layer and a heat generating porous layer has been investigated numerically.

For a fixed aspect ratio $A = 2$, two groups of steady solutions with different flow patterns and heat transfer performance were found by adapting the pseudo arc-length continuation method with tilt angle as the continuation parameter. The first group lies in between $\varphi = 0^\circ$ and 360°. At any tilt angle, the flow pattern of this group is either a single cell or two cells. The second group of solutions exist between $\varphi = 0^\circ$ and a extreme turning angle which varies with the Rayleigh number. The flow patterns of this group consist of multiple cells.

The effects of aspect ratio on the flow patterns and heat transfer performance for the case of $\varphi = 0^\circ$ have also been studied. It has been shown that the global Nusselt number increases with increasing aspect ratio for flows of similar pattern with the same number of cells.

The sensitivity of the porosity as well as the Darcy number on flow are also investigated. According to our study, both of the effects has small influence on flow.

References

1. **Prasad, V.:** Thermal convection in a rectangular cavity filled with a heat-generating, Darcy porous medium. J. Heat Transfer 109 (1987) 697–703
2. **Rao, Y. F.; Wang B. X.:** Natural convection in vertical porous enclosures with internal heat generation. Int. J. Heat Mass Transfer 34 (1991) 247–252
3. **Stewart, W. E.; Dona, C. L. G.:** Free convection in a heat-generating porous medium in a finite vertical cylinder. J. Heat Transfer 110 (1988) 517–520
4. **Royer, J. J.; Flores, L.:** Two-dimensional natural convection in an anisotropic and heterogeneous porous medium with internal heat generation. Int. J. Heat Mass Transfer 34 (1994) 1387–1399
5. **Weinitschke, H. J.; Nandakumar, K.; Sanker, S. R.:** A bifurcation study of convective heat transfer. Phys. Fluid A 2 (1990) 912–921
6. **Viljoen, H.; Hlavacek, V.:** Chemically driven convection in a porous medium. A.I.Ch.E. J1 33 (1987) 1344–1350
7. **Subramanian, S.; Balakotaiah, V.:** Mode interactions in reaction-driven convection in a porous medium. Chem. Eng. Sci. 50 (1995) 1851–1866
8. **Inaba, H.; Sugawara, M.; Blumenberg, J.:** Natural convection heat transfer in an inclined porous layer. Int. J. Heat Mass Transfer 31 (1988) 1365–1374
9. **Moya, S. L.; Ramos, E.; Sen, M.:** Numerical study of natural convection in a tilted rectangular porous material. Int. J. Heat Mass Transfer 30 (1987) 741–756
10. **Vasseur, P.; Satish, M. G.; Robillard, L.:** Natural convection in a thin, inclined, porous layer exposed to a constant heat flux. Int. J. Heat Mass Transfer 30 (1987) 537–549
11. **Sen, M.; Vasseur, P.; Robillard, L.:** Multiple steady states for unicellular natural convection in an inclined porous layer. Int. J. Heat Mass Transfer 30 (1987) 2097–2113
12. **Vafai, K.; Thiyagaraja, R.:** Analysis of flow and heat transfer at the interface region of a porous medium. Int. J. Heat Mass Transfer 30 (1987) 1391–1405
13. **Beckermann, C.; Viskanta, R.; Ramadhyani, S.:** Natural convection in vertical enclosures containing simultaneously fluid and porous layers. J. Fluid Mech. 186 (1988) 257–284
14. **Chen F.; Chen, C. F.:** Convection in superposed fluid and porous layers. J. Fluid Mech. 234 (1992) 97–119

15. **Kim, S. J.; Choi, C. Y.:** Convective heat transfer in porous and overlaying fluid layers heated from below. Int. J. Heat Mass Transfer 39 (1996) 319–329
16. **Nishimura, T.; Takumi, T.; Shiraishi, M.; Kawamura, Y.; Ozoe, H.:** Numerical analysis of natural convection in a rectangular enclosure horizontally divided into fluid and porous regions. Int. J. Heat Mass Transfer 29 (1986) 889–898
17. **Poulikakos, D.:** Thermal instability in a horizontal fluid layer superposed on a heat-generating porous bed. Num. Heat Transfer 12 (1987) 83–99
18. **Keller, H. B.:** Numerical solution of bifurcation and nonlinear eigenvalue problems, in: Applications of Bifurcation Theory. (Ed. by P. H. Rabinowiz) New York: Academic 1977
19. **Vafai, K.; Tien, C. L.:** Boundary and inertia effects on flow and heat transfer in porous media. Int. J. Heat Mass Transfer 24 (1981) 195–203
20. **Neale, G.; Nader, W.:** Practical significance of Brinkman extension of Darcy law: coupled parallel flows within a channel and boundary porous medium. Can. J. Chem. Engng. 52 (1974) 472–478
21. **Lundgren, T. S.:** Slow flow through stationary random beds and suspensions of spheres. J. Fluid Mech. 51 (1972) 273–299
22. **Lauriat, G.; Prassad, V.:** Non-Darcian effects on natural convection in a vertical porous enclosure. Int. J. Heat and Mass Transfer 32 (1989) 2135–2147
23. **Patankar, S.:** Numerical Heat Transfer and Fluid Flow. New York: Hemisphere 1980
24. **Saad, Y.; Schultz, M. H.:** Gmres – A generalized minimal residual algorithm for solving non symmetric linear-systems, SIAM J. Sci. Stat. Comput. 7 (1986) 856–869
25. **Fletcher, C. A. J.:** Computational Techniques for Fluid Dynamics II. New York: Springer 1991
26. **Nield, D. A.; Bejan, A.:** Convection in Porous Media. New York: Springer 1992